Soil & Tillage Research 165 (2017) 239–246

Contents lists available at ScienceDirect

Soil & Tillage Research

journal homepage: www.elsevier.com/locate/still

Quantification of soil aggregate microstructure on abandoned cropland during vegetative succession using synchrotron radiation-based micro-computed tomography

Dong Zhao[a,c], Mingxiang Xu[a,b], Guobin Liu[a,*], Xu Yao[b], Dengfeng Tuo[b], Rongrong Zhang[b], Tiqiao Xiao[d], Guanyun Peng[d]

[a] State Key Laboratory of Soil Erosion and Dryland Farming on the Loess Plateau, Institute of Soil and Water Conservation, Chinese Academy of Sciences and Ministry of Water Resources, Yangling, Shaanxi 712100, PR China
[b] Northwest A & F University, Yangling, Shaanxi 712100, PR China
[c] University of Chinese Academy of Sciences, Beijing 100049, PR China
[d] Shanghai Synchrotron Radiation Facility (SSRF), Shanghai Institute of Applied Physics, Chinese Academy of Science, Shanghai 201204, PR China

ARTICLE INFO

Article history:
Received 26 March 2016
Received in revised form 15 July 2016
Accepted 11 August 2016
Available online xxx

Keywords:
Aggregate microstructure
Abandoned cropland
Micro-computed tomography

ABSTRACT

Information for the microstructure of soil aggregates is crucial for understanding the mechanisms of various soil processes. The quantification of complex aggregate microstructure and its relationship to vegetative restoration, however, remains elusive. The objective of this study was to evaluate the impact of natural revegetation on aggregate microstructure using synchrotron-based X-ray micro-computed tomography and image analysis. Soil samples were collected from an active cropland and from four former croplands that have been abandoned for 6, 12, 23, and 32 years on the Loess Plateau, China. Soil aggregates (3–5 mm) were scanned at a voxel resolution of 3.25 μm, and the aggregate pore structure was visualized and quantified with ImageJ software. The stability of wet aggregates and other soil properties were also evaluated. The amount of soil organic carbon increased significantly and soil bulk density decreased significantly with abandonment age. Aggregate water stability was higher after revegetation but did not differ significantly among the abandoned sites. Total porosity, percentage of pores >75 μm, and the fraction of elongated pores increased, but the number of pores, percentage of pores <75 μm, and fractions of regular and irregular pores decreased after the croplands were abandoned. The fractal dimension, degree of anisotropy and the Euler number all indicated that aggregate microstructures were more connected and developed at all abandoned sites than in the active cropland, but the fractal dimension was more sensitive for monitoring the quality of the soil structure. The results from this study can help to improve our understanding of the soil processes during natural vegetative succession and of the importance of pore morphology in monitoring the quality of soil structure.

1. Introduction

Soil structure plays a key role in determining the retention and transport of water, gases, and nutrients in soils, preserving soil productivity, and maintaining soil porosity and resistance to erosion (Barthès and Roose, 2002; Miller and Jastrow, 1990; Rillig and Mummey, 2006; Six et al., 2000). Soil structure can be broadly defined by form and stability (Bronick and Lal, 2005). Soil aggregates, i.e. clusters of soil particles that adhere to each other more strongly than to other surrounding particles (Barto et al., 2010), are widely regarded as principal soil structural units. Studies of soil structure usually focus on aggregate stability, size, and turnover (Bronick and Lal, 2005; Six et al., 2004; Kavdır and Smucker, 2005), ignoring the internal microstructure of aggregates. Aggregate stability has particularly been widely used to evaluate the stability of soil structure but cannot provide information about the status of aggregate structure (Young et al., 2001). The microstructure of soil aggregates determines soil stability and quality (Zhou et al., 2013), so information on the microstructure of aggregates can be essential for understanding the status and processes of soil structure.

* Corresponding author.
E-mail address: gbliu@ms.iswc.ac.cn (G. Liu).

http://dx.doi.org/10.1016/j.still.2016.08.007
0167-1987/

The direct investigation of aggregate structure has generally relied on the observation and quantification of thin sections or blocks using light microscopy, electron microscopy, and digital image analysis (Pagliai et al., 2004; Perfect and Kay, 1995; Zhou et al., 2012). These methods provide limited and fragmented information for aggregation structure, partly due to the lack of reliable methods for non-destructive observation and 3D measurements at an appropriate scale (Garbout et al., 2013a). These approaches also use destructive sampling and can be very laborious. The traditional methods have recently been supplemented with advanced nondestructive X-ray computed tomography (CT) scanning technology, which has the advantage of higher resolution and contrast and faster scanning (Garbout et al., 2012, 2013a, 2013b; Taina et al., 2008). Micro-CT, especially synchrotron radiation-based micro-computed tomography (SR-μCT), in combination with image analysis, can provide not only 3D data of porosity and pore-size distribution, but can also quantify and visualize pore orientation and complexity (Dal Ferro et al., 2013; Peth et al., 2008). Kravchenko et al. (2011), quantifying the effects of tillage on intra-aggregate porosity using micro-X-ray CT, indicated that long-term differences in land use and management practices may lead to substantial differences in intra-aggregate pore distributions and structures. Dal Ferro et al. (2013), using micro-X-ray CT to assess the effect of soil organic carbon (SOC) on the pore network of both undisturbed soil cores and aggregates, reported that SOC strongly affected the pore-size distribution in soil cores but weakly affected the pore network at an aggregate scale. These authors also suggested that morphological features such as connectivity were effective indices for differentiating the effects of management practices. Few studies, however, have specifically applied X-ray CT to visualize and quantify the influence of vegetative rehabilitation, particularly natural revegetation, on an aggregate microstructure.

The Loess Plateau in China covers approximately 58×10^4 km^2, has a typical semiarid climate, and is known for its long agricultural history and serious soil erosion (Chen et al., 2007). Many erosion-prone slopes and sandy native grasslands have been converted into farmland to provide food security under the pressures of a growing population (Wei et al., 2006; Zhang et al., 2011), which produced serious soil deterioration due to erosion (Turner et al., 2011). Efforts have been undertaken to restore the eroded land by reconverting croplands into grasslands, such as the 'Grain for Green' project (An et al., 2013; Zhang et al., 2013). This conversion has increased the coverage of vegetation by the natural colonization of the abandoned fields by the surrounding natural vegetation (Wang et al., 2009; Zhang et al., 2012). The re-establishment of natural species-rich heaths on abandoned farmland is one of the main measures for controlling soil erosion on the plateau (Wang et al., 2011a). Abandoned croplands that have been stabilized by natural vegetation for different lengths of time thus offer a good opportunity for studying the mechanisms affecting soil structure during natural vegetative succession on the plateau.

We hypothesized that natural revegetation on abandoned cropland would improve the stability of soil aggregates, which would likely stabilize after several years of restoration. We also hypothesized that the microstructure of soil aggregates would become more connected and complex during natural revegetation. The objectives of this study were thus to (1) evaluate the effect of vegetative restoration on aggregate stability and (2) visualize and quantify the 3D aggregate microstructure with high resolution SR-μCT and image analysis during natural vegetative succession.

2. Materials and methods

2.1. Site description

The study was conducted in the Zhifanggou Watershed at the Ansai Research Station of Soil and Water Conservation in Shaanxi Province, northern Loess Plateau, China (109°13′46″–109°16′33″E, 36°43′11″–36°46′25″N; 1010–1431 m a.s.l.; 8.27 km^2). The climate in this area is temperate semiarid, with a mean annual temperature of 8.8 °C (min −23.6 °C and max 36.8 °C) and a mean annual precipitation of 505 mm, about 70% of which falls between July and September. The annual evaporation ranges from 1010 to 1400 mm, and the average frost-free period is approximately 157 days. The soil at the study site was primarily Huangmian soil (Calcaric Cambisol, FAO, 1990), originating from wind deposits and characterized by a yellow color, absence of bedding, silty texture, and looseness (Zhang et al., 2011).

2.2. Experimental design and soil sampling

A common approach in studies of the effect of soil rehabilitation on vegetative coverage is to monitor changes in the plants and soil along a successional chronosequence on similar soils under similar climatic conditions (Bhojvaid and Timmer, 1998). Substituting space for time is an effective way to study changes over time (Li et al., 2007; Sparling et al., 2004). The Zhifanggou watershed has been protected for more than 30 years to allow natural

Table 1
Geographical features and vegetation characteristics of the sampling sites.

Plot name	Abandoned cropland (years)	Elevation (m)	Slope gradient	Geographical coordinates ψ(N), λ(E)	Dominant species	Accompanying species
Cr	0	1266	19°	36°44′39″ 109°14′35″	*Setaria italica*	
AC.6	6	1292	23°	36°44′47″ 109°15′12″	*Artemisia capillaries* Thunb *Heteropappus altaicus*	*Potentilla bifurca* L. *Lespedeza davurica* (Laxm.) *Poa annua* L. *Cleistogenes squarrosa* (Trin.)
AC.12	12	1289	21°	36°44′02″ 109°16′31″	*Artemisia capillaries* Thunb *Artemisia sacrorum* Ledeb	*Stipa bungeana* Trin *Heteropappus altaicus* *Poa annua* L. *Lespedeza davurica* (Laxm.) Schindl
AC.23	23	1283	23°	36°44′05″ 109°16′27″	*Stipa bungeana* Trin *Artemisia sacrorum Ledeb*	*Salsola collina* *Lespedeza davurica (Laxm.)Schindl* *Potentilla bifurca L.*
AC.32	32	1325	28°	36°44′15″ 109°15′55″	*Artemisia sacrorum Ledeb*	*Stipa bungeana* *Trin Vicia sepium L.* *Patrinia heterophylla Bunge*

Note: Cr—slope cropland; AC.6, AC.12, AC.23, AC.32—abandoned croplands for 6, 12, 23, 32 years.

revegetation (Wang et al., 2011a). We selected an active cropland (Xue et al., 2013) to serve as a control and four former croplands that had been abandoned for 6, 12, 23, and 32 years as the experiment sites. The ages of the abandoned croplands were established from inquiries of the local villagers and from land documents. The sampling sites were all near the tops of loessial mounds and differed little in aspect, slope gradient, elevation, and previous farming practices. The abandoned sites were maintained under natural conditions with little human disturbance. The main crops grown in the active cropland were millet (*Setaria italica*) and soybean (*Glycine max*). One crop was grown each year, and fertilizer was applied before planting. The cropland was ploughed in the spring to 20–25 cm depth using a hoe and a plow for more than 40 years. At the time of sampling, the arable field was in the year of the millet phase. Detailed information on the sample sites is shown in Table 1.

Soil samples were collected from the top layer (0–15 cm) in May 2014 and carefully transported to the laboratory. An area of $100 \times 100\,m^2$ was randomly selected at each site, and five $20 \times 20\,m^2$ plots were established within this area for sampling. Soil samples were collected from five points at each plot to make a composite sample for each replicate after thorough mixing. Five undisturbed soil cores were collected at each site using cylindrical stainless-steel samplers (5 cm in length and 7 cm in diameter) from the 5–15 cm layer for determining the bulk density at each site. The samples were air-dried in the laboratory at room temperature and then divided into two subsamples. One subsample was sieved to determine soil physicochemical properties using routine methods. Soil organic carbon (SOC) content was determined by oxidation with potassium dichromate in a heated oil bath (Soil Survey Laboratory Methods Manual, 2004), and soil texture was determined using a Malvin Laser Particle Size Analyzer (Mastersizer 2000, Malvern Instruments Ltd, Worcestershire, UK). The other subsample was used to select 3–5 mm aggregates for determining aggregate water stability and for SR-μCT scanning. Five aggregates were randomly selected from each sample for the SR-μCT study due to the limitation of beam time. The selected aggregates were oven-dried at 40 °C for 24 h and stored at 4 °C before CT scanning.

2.3. CT scanning and image processing

Images were acquired using the BL13W1 beamline of the Shanghai Synchrotron Radiation Facility (SSRF). The aggregate samples were scanned at 24 keV with an 1800 ms exposure and a distance of 12 cm between the X-ray gun and the sample, generating an axial sequence of X-ray attenuation images. After scanning, the filtered back-projection algorithm was used to reconstruct slices from the radiographs. About 550 slices with a size of 2048×2048 pixels for each slice were reconstructed for each sample. Each voxel represented a volume of $3.25 \times 3.25 \times 3.25\,\mu m$, where the voxel-associated attenuation coefficients were stored as grayscale values ranging from 0 (lowest attenuation) to 255 (highest attenuation).

The images were processed, visualized, and quantified using the open-source software ImageJ, ver. 1.48 v (Rasband, 1997–2014). Ring artifacts in some slices were removed before image segmentation (Zhou et al., 2013). Examples of the grayscale slices are shown in Fig. 1. Image segmentation into pores and solids is a crucial step in most analyses of soil images. Segmentation of the grayscale slices was performed using the automatic Otsu thresholding algorithm (Garbout et al., 2013a; Wang et al., 2011b), and resulted in binary images from the original grayscale images. The binary images were subsequently analyzed.

Sub-volumes of $500 \times 500 \times 500$ voxels, representing an inscribed cube of an aggregate, were extracted for further analysis to avoid edge effects. The 3D aggregates were volume-rendered

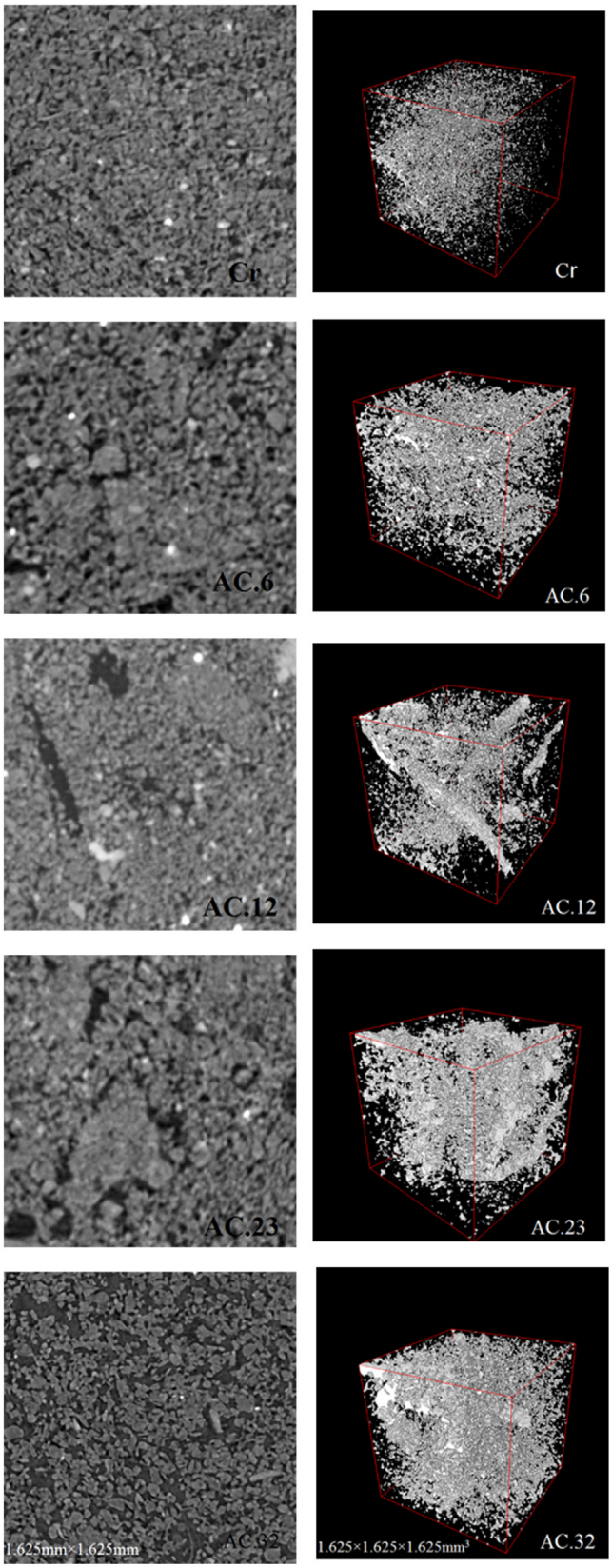

Fig 1. Representative 2D (left) and 3D (right) visualizations of soil aggregate structures as a result of SR-μCT on abandoned cropland during vegetative succession.
Note: Cr—slope cropland; AC.6, AC.12, AC.23, AC.32—abandoned croplands for 6, 12, 23, 32 years.

and visualized with the ImageJ 3D viewer plug-in (Schmid et al., 2010); examples are shown in Fig. 1. The characteristics of the soil pore structure (i.e. porosity, pore-size distribution, and pore surface area) of the 3D images were generated using the ImageJ 3D object counter plug-in (Bolte and Cordelieres, 2006). Pore sizes were expressed as equivalent diameters, and the pores were classified into four size classes based on their equivalent diameter: <30 μm, 30–75 μm, 75–100 μm, and >100 μm (Ma et al., 2015).

2.4. Pore morphology

The pore-shape factor (F) was calculated as (Wadell, 1932):

$$F = \frac{A_e}{A} \quad (1)$$

where A_e is the surface area of a sphere with a volume equal to that of the pore, and A is the measured area of the pore surface. F is 1 for a sphere and <1 for more irregular or elongated pore shapes. We classified pores as regular ($F \geq 0.5$), irregular ($0.2 < F < 0.5$), or elongated ($F \leq 0.2$) following the method of Zhou et al. (2012).

The three-dimensional mass fractal dimension (FD) is used to describe objects that possess self-similarity and scale-independent properties and increases with structural complexity (Dal Ferro et al., 2013). FD was calculated following the box-counting method of covering the image stack with various cube sizes and recording the number of boxes ($N(\delta)$) intersecting the pores within the stack (Kravchenko et al., 2011; Perret et al., 2003). FD can thus be estimated by the linear regression of $\log\{N(\delta)\}$ against $\log(1/\delta)$ for numbers between 2 and 3. FD was calculated using the ImageJ plug-in Fractal Count (Dal Ferro et al., 2013; Ersoy et al., 2008).

We evaluated the orientation and connectivity of soil-pore networks, degree of anisotropy (DA), and connectivity using the ImageJ plug-in BoneJ (Doube et al., 2010). The 3D DA is a calculated geometric characteristic (Odgaard, 1997), because preferential alignment along an axis can have a large impact on transport. DA varies between 0 (perfect isotropic structure) and 1 (anisotropic structure). The 3D connectivity of pores was quantified with the volumetric Euler-Poincaré characteristic (Deurer et al., 2009) (hereafter Euler number, or E_v). The larger the E_v, the lower the connectivity of the pore system. The theoretical background and methodological details of the image analysis for deriving DA and E_v are available elsewhere (Dal Ferro et al., 2013).

2.5. Stability of wet aggregates

Stability tests used the Le Bissonnais (1996) method and the fast-wetting treatment. Aggregates of 3–5 mm in diameter were oven-dried at 40 °C for 24 h prior to the wet-aggregate stability test to establish a constant matric potential. Five grams of the dried aggregates were immersed in distilled water for 10 min, and the water was then removed with a pipette. Fragments <50 μm were separated from those >50 μm by gently sieving through a 50-μm mesh five times. The >50 μm fraction was collected, oven-dried, and gently dry-sieved through a column of six sieves: 2000, 1000, 500, 200, 100, and 50 μm.

The wet-aggregate stability for the fragment sizes was expressed as the mean weight diameter (MWD):

$$MWD - \sum_{1}^{n+1} \frac{r_{i-1} - r_i}{2} \times m_i \quad (2)$$

where r_i is the aperture of the ith mesh (μm), $r_0 = r_1$ and $r_n = r_{n+1}$, m_i is the weight fraction of the aggregates on the ith sieve, and n is the number of sieves.

2.6. Statistical analysis

The results are expressed as means ± standard deviations. Significant differences in aggregate stability and pore characteristics among the sites were analyzed using a one-way analysis of variance and Fisher's protected least significant difference test. Pearson correlation analysis was used to determine the relationships between SOC content, clay content, and pore characteristics. All statistical analyses used SPSS version 20.0 (SPSS Inc. Chicago, USA) at $P = 0.05$.

3. Results and discussion

3.1. Soil properties

Soil quality on abandoned land can recover by restoring the native vegetation (Wang, 2002; Wang et al., 2011a). Many soil properties changed considerably with abandonment age (Table 2). SOC content increased significantly and bulk density decreased significantly ($P < 0.05$) during the natural vegetative succession. Tillage practice often increases the air exchange and oxygen availability, resulted in enhancement of the decomposition of organic matter (An et al., 2013). The conversion of cropland to abandoned cropland, with no tillage practice and the increase of the inputs of plant residues, has resulted in the enrichment of SOC (Rutigliano et al., 2004). Increasing aboveground biomass during succession also increases belowground biomass (roots), which decreases soil bulk density (Jiang et al., 2009). The texture of the surface soil did not differ significantly among the sites ($P > 0.05$).

MWD, as the most important index of aggregate stability, was lower at the cropland site than the abandoned sites. Tillage causes changes in soil structure by direct physical disturbance due to plowing, disrupting soil aggregates in a manner that leads to reduction in the aggregates stability (Park and Smucker, 2005). The differences of MWD between the abandoned sites, however, were small, with no obvious changes ($P > 0.05$), indicating that aggregate stability had reached a steady state after six years of abandonment. This finding is consistent with that by An et al. (2013), who found that high aggregate stabilities were reached after three and seven years under afforestation and non-grazed grassland on the Loess Plateau, respectively. Soil texture, especially clay content, did not

Table 2
Soil physical and chemical properties during succession of abandoned cropland.

	Sand (%)	Silt (%)	Clay (%)	SOC(g kg^{-1})	BD(g cm^{-3})	MWD(mm)
Cr	61.7 ± 1.9 a	27.6 ± 2.7 a	10.7 ± 0.8 a	3.04 ± 0.38 c	1.18 ± 0.02 a	1.03 ± 0.33 b
AC.6	62.5 ± 4.3 a	27.3 ± 3.2 a	10.2 ± 1.2 a	4.37 ± 0.94 b	1.13 ± 0.09 ab	1.95 ± 0.29 a
AC.12	64.0 ± 4.9 a	25.8 ± 3.6 a	10.1 ± 1.4 a	4.21 ± 0.81 ab	1.14 ± 0.04 ab	2.19 ± 0.21 a
AC.23	62.8 ± 3.4 a	26.9 ± 3.1 a	10.2 ± 1.0 a	4.65 ± 0.13 b	1.09 ± 0.02 bc	2.17 ± 0.21 a
AC.32	65.6 ± 1.4 a	24.5 ± 1.1 a	9.9 ± 0.5 a	5.90 ± 0.73 a	1.05 ± 0.04 c	2.49 ± 0.22 a

Note: SOC, soil organic carbon; BD, bulk density; MWD, mean weight diameter. Results are given as mean ± SD. Different letters following values in the same column indicate significant difference at the 0.05 level (LSD).

Table 3
General properties of soil pore network of the aggregates in the different sites.

	Cr	AC.6	AC.12	AC.23	AC.32
Total porosity	14.1 ± 1.1 d	15.4 ± 0.4 cd	16.6 ± 0.9 bc	16.9 ± 0.5 b	20.5 ± 1.8 a
Total number of pores	18739 ± 2596 a	10114 ± 3009 b	7445 ± 635 c	6287 ± 665 cd	4140 ± 350 d
Fractal dimension(FD)	2.74 ± 0.03 d	2.77 ± 0.05 cd	2.80 ± 0.05 bc	2.82 ± 0.03 ab	2.86 ± 0.02 a
Degree of anisotropy(DA)	0.21 ± 0.03 b	0.29 ± 0.05 a	0.28 ± 0.02 a	0.34 ± 0.04 a	0.31 ± 0.06 a
Euler number (10^{-5} pixel^{-3})(E_v)	7.4 ± 2.9 a	2.0 ± 0.8 b	3.8 ± 1.8 b	2.0 ± 0.8 b	3.6 ± 1.8 b
Largest pore/volume total porosity (%)	82.4 ± 4.2 c	84.4 ± 2.9 bc	88.4 ± 1.7 b	87.4 ± 4.4 b	93.4 ± 1.5 a
Mean shape factor(F)	0.61 ± 0.01 a	0.58 ± 0.03 b	0.57 ± 0.01 b	0.47 ± 0.01 c	0.43 ± 0.01 d

Note: Different letters following values within a row indicate significant difference at the 0.05 level (LSD).

differ significantly between the sites, implying that the significant variation of aggregate water stability was mainly due to the improvement of soil structure and to increases in SOC content during the recovery (Li and Shao, 2006). A positive correlation between MWD and SOC content was found (Table 4). Pulleman and Marinissen (2004) reported that the water stability of aggregates is low in arable soils compared to grassland soils, and decreases with SOC content of the soil. Enrichment in SOC, mainly hydrophobic organic compounds, can increase water repellency during vegetative restoration, which will reduce slaking stresses and entrapped air pressure, thereby increasing aggregate water stability (Peng et al., 2003).

3.2. Porosity and pore-size distribution of soil aggregates

Aggregate microstructure was modified substantially during the succession (Table 3). The porosity of the aggregates increased by approximately 9.2, 18.1, 19.9, and 45.9% relative to the cropland site at AC.6, AC.12, AC.23, and AC.32, respectively. Tillage can increase wetting–drying cycles of soils (Smucker et al., 2007), resulting in more microcracks formation and a decrease in porosity accordingly. Conversely, the pore number decreased significantly with abandonment age, which may have been due to the increase in roots that exploit cracks, voids, and large pores or enlarge smaller pores by displacing soil particles (Clark et al., 2003). Most of the porosity was attributed to the larger pores (Fig. 2). Organic carbon was positively correlated with the porosity and negatively correlated with the number of pores (Table 4). The amount of organic matter increased with abandonment age, which can positively affect the porosity, as demonstrated by Emerson and McGarry (2003).

The distribution of pore sizes is shown in Fig. 2. Approximately 88% of the aggregate porosity was represented by pores >100 μm, and this proportion increased with abandonment age. A higher percentage of large pores increases water infiltration and drainage and stabilizes the soil structure (Dal Ferro et al., 2013). The porosity for diameters <30 μm and 30–75 μm decreased considerably, and the porosity for diameters 75–100 μm increased to a lesser extent. The pore-size distribution, however, was nearly identical among AC.6, AC.12, and AC.23. In contrast, the porosity for diameters >75 μm increased at AC.32 by approximately 59%, whereas the <75 μm porosity decreased by 66% relative to the cropland. SOC content was positively correlated with >75 μm porosity and negatively correlated with 30–75 μm porosity. These results are partially consistent with those by Zhou et al. (2013), who observed that the porosity of Ultisol aggregates with diameters >50 μm increased significantly after vegetative restoration. These authors also found that <50 μm porosity was nearly identical between bare land and revegetated land. In contrast, Kravchenko et al. (2011) indicated that small-pore (15–60 μm) porosity was lowest in abandoned cropland and highest in conventionally tilled cropland. They suggested that the decrease in small-pore porosity in abandoned cropland could be due to a higher SOC content, because SOC can enter macro-aggregates through intra-aggregate pores and serve as a binding agent preventing the formation of microcracks, thus leading to fewer small pores. These contradictory results are likely due to the different soil types.

Table 4
Correlation coefficient matrix of soil aggregate parameters and selected physico-chemical characteristics.

	Clay	SOC
Total porosity	−0.22	0.62**
Total number of pores	0.15	−0.69**
<30 μm porosity	0.37	−0.27
30–75 μm porosity	0.24	−0.60**
75–100 μm porosity	−0.18	0.43*
>100 μm porosity	−0.21	0.61**
Fraction of regular pores (%)	0.16	−0.52**
Fraction of irregular pores (%)	0.23	−0.47*
Fraction of elongated pores (%)	−0.21	0.57**
FD	−0.33	0.73**
DA	−0.44*	0.33
E_v	−0.17	−0.40
MWD	−0.16	0.63**

* $P < 0.05$.
** $P < 0.01$.

3.3. Pore morphology of the soil aggregates

Natural revegetation after cropland abandonment strongly affected pore shape (Fig. 3). The fractions of elongated pores, which are very important for the storage and transmission of soil water and gases (Pagliai et al., 2004), were dominant (on average 80%) in all samples from the abandoned sites, with a tendency to increase during natural vegetative succession. In contrast, the fractions of regular and irregular pores were significantly lower at the abandoned sites than at the cropland site. An increase in cracked and elongated pores at the abandoned sites, especially AC.32, was also evident from visual observations as shown in Fig. 1. Zhou et al. (2013) similarly reported that the percentage of elongated pores was significantly higher in treatments with restored vegetation than in the control. SOC content was correlated positively with the fractions of elongated pores but negatively with the fractions of regular and irregular pores (Table 4). F decreased significantly ($P < 0.05$) during the succession on the abandoned croplands (Table 3).

FD changed slightly with abandonment age (Table 3) but was only 4.6% higher at AC.32 than at the cropland site, likely due to the large differences in pore morphology (Fig. 1). SOC was positively correlated with FD (r = 0.73) (Table 4). FD was higher in the abandoned sites than in the cropland site, indicating greater pore heterogeneity and complexity after revegetation (Kravchenko et al., 2011; Zhou et al., 2013). We found a curvilinear relationship between porosity and FD (Fig. 4), as have other studies (Dal Ferro et al., 2013; Perret et al., 2003), suggesting that the effect on pore complexity could be mostly attributed to porosity due to image resolution (De Gryze et al., 2006). The greater complexity of the pore system is expected to be beneficial for the aeration of microsites within the soil (Garbout et al., 2013a).

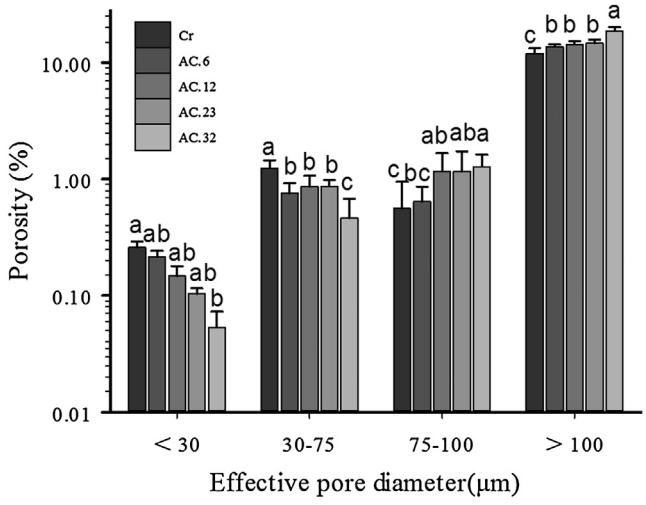

Fig. 2. Pore-size distributions of soil aggregates from the different treatments. *Note*: Different letters following values between different successional stages indicate significant difference at the 0.05 level (LSD). Error bars indicate standard errors.

DA was higher in the abandoned croplands (average 0.29) than the active cropland (average 0.21), indicating that the pore network became better oriented and could be more conducive to the movement of water, solutes, and air (Horn and Smucker, 2005). Conversely, DA did not differ significantly between the abandoned sites ($P > 0.05$) (Table 3). The largest pores within the aggregates accounted for averages of 82 and 88% of the total porosity for the cropland site and the abandoned sites, respectively, indicating that more direct pathways were provided to the soil surface. E_v averaged 7.4×10^{-5} pixel^{-3} in the cropland aggregates and 2.8×10^{-5} pixel^{-3} in the abandoned-cropland aggregates. The connectivity of the soil aggregates increased significantly after abandonment, and E_v decreased but did not differ significantly between the abandoned sites ($P > 0.05$) (Table 3). Zhou et al. (2013) also reported that the microstructure of soil aggregates developed from a very dense massive microstructure to a more porous microstructure after two decades of vegetative restoration.

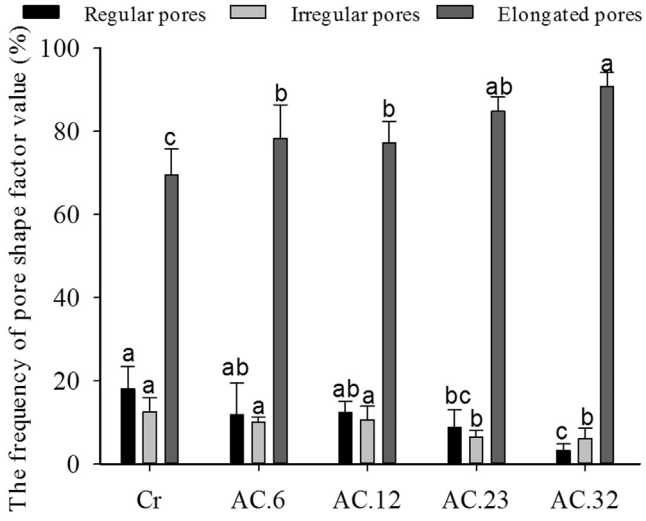

Fig. 3. Pore shape distribution of soil aggregates in different treatments. *Note*: Different letters following values between different successional stages indicate significant difference at the 0.05 level (LSD). Error bars indicate standard errors.

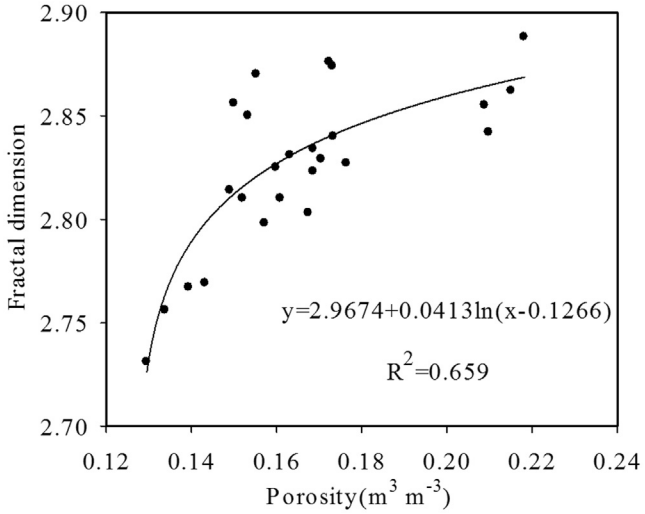

Fig. 4. Relationship between fractal dimension (FD) and total porosity of soil aggregates.

3.4. Time evolution of MWD and pore network

In general, the aggregate stability was represented by a curve, with a rapid increase after abandonment ($P < 0.05$), and relative constant after 6 years of abandonment ($P > 0.05$) (Fig. 5). However, the porosity of the aggregates significantly increased from 0 to 12 years of restoration ($P < 0.05$), and remained stable between 12 years and 23 years ($P > 0.05$), then increased from years 23 through 32 ($P < 0.05$). From 6 to 32 years of restoration, MWD indicated that aggregate stability reached relative constant, however, porosity showed the soil microstructure was continually changing. Neither DA nor E_v differed significantly between the abandoned sites, even though pore-size distribution, F, and FD provided evidence that pore tortuosity and complexity differed at the sites, which indicated that pore-size distribution, F, and FD were more sensitive than DA and E_v to the stages of revegetation from 6 to 32 years. Pore-size distribution, F, and FD should thus be regarded as better indicators of the quality of soil structure.

Soil structure provides pathways for the transport of water, nutrients, and gases and habitats for microorganisms and fauna and so is a fundamental property of soil fertility and quality (Peng et al., 2015). The recovery of soil structure by restoring vegetation

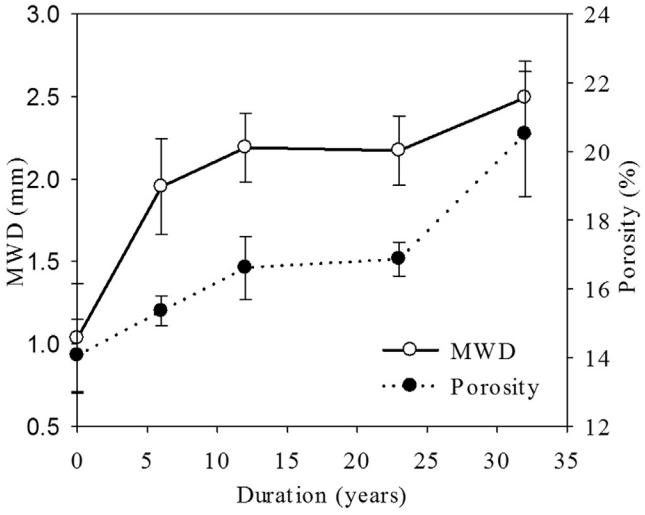

Fig. 5. Time evolution of MWD and total porosity of soil aggregates.

on abandoned land is thus key to improving soil quality and fulfilling essential soil functions. The absence of tillage and increase in root growth by the restoration of vegetation contributed most to improving soil structure, but other factors such as soil biological activity also likely contributed (Zhao et al., 2010). Aggregate water stability on the Loess Plateau remained nearly constant after six years of revegetation on the abandoned cropland, but the soil microstructure continued to develop toward a more connected and porous form, which can lead to the gradual recovery of other soil functions, such as saturated hydraulic conductivity and the capacity of soil to retain water (Li and Shao, 2006). In further studies, we will combine CT and image analysis with physicochemical methods to evaluate the effects of the different microstructures on soil hydraulic functions during natural vegetative succession.

4. Conclusions

We investigated the three-dimensional microstructural characteristics of soil aggregates on abandoned cropland during vegetative succession using SR-μCT and image analysis. Aggregate water stability on the abandoned cropland peaked after six years of revegetation. Revegetation significantly affected the pore-size distribution, with a shift from small (<75 μm) to larger (>75 μm) pores. Total porosity, the fraction of elongated pores, FD, DA, and connectivity increased, and the number of pores and the fractions of regular and irregular pores decreased after the cropland was abandoned. These quantitative results, together with the 2D and 3D observations, indicated that aggregate microstructures were more developed at the sites of abandoned cropland than at the active cropland site. The improvement of the soil microstructure was rapid right after the abandonment, and slowed down after 6 years of abandonment.

Based on CT scanner image analysis, the measurement of morphometric parameters has the potential to provide new fundamental insight into the quantification of soil aggregate structure. CT should be more widely used in combination with other methods to investigate soil microstructure and explore the mechanisms of soil aggregation in order to improve our understanding of soil processes.

Acknowledgments

This work was supported by the Special Program for Basic Research of the Ministry of Science and Technology, China (2014FY210100), the Key Research Program of the Chinese Academy of Sciences (KJZD-EW-TZ-G10), and the National Natural Science Foundation of China (41171422). We thank the Shanghai Synchrotron Radiation Facility (SSRF) for supporting the use of the radiation source Dr. Yudan Wang from the BL13W1 beam line of SSRF for their helpful instruction. We thank Associate Professor Hu Zhou of the Institute of Soil Science, Chinese Academy of Science for quantitative image analysis for his assistance.

References

An, S.S., Darboux, F., Cheng, M., 2013. Revegetation as an efficient means of increasing soil aggregate stability on the Loess Plateau (China). Geoderma 209, 75–85.
Barthès, B.G., Roose, E., 2002. Aggregate stability as an indicator of soil susceptibility to runoff and erosion; validation at several levels. Catena 47, 133–149.
Barto, E.K., Alt, F., Oelmann, Y., Wilcke, W., Rillig, M.C., 2010. Contributions of biotic and abiotic factors to soil aggregation across a land use gradient. Soil Biol. Biochem. 42, 2316–2324.
Bhojvaid, P., Timmer, V., 1998. Soil dynamics in an age sequence of Prosopis juliflora planted for sodic soil restoration in India. Forest Ecol. Manag. 106, 181–193.
Bolte, S., Cordelieres, F., 2006. A guided tour into subcellular colocalization analysis in light microscopy. J. Microsc. Oxford 224, 213–232.
Bronick, C.J., Lal, R., 2005. Soil structure and management: a review. Geoderma 124, 3–22.
Chen, L.D., Gong, J., Fu, B.J., Huang, Z.L., Huang, Y.L., Gui, L.D., 2007. Effect of land use conversion on soil organic carbon sequestration in the loess hilly area, Loess Plateau of China. Ecol. Res. 22, 641–648.
Clark, L.J., Whalley, W.R., Barraclough, P.B., 2003. How do roots penetrate strong soil? Roots: The Dynamic Interface Between Plants and the Earth. Springer, pp. 93–104.
Dal Ferro, N., Charrier, P., Morari, F., 2013. Dual-scale micro-CT assessment of soil structure in a long-term fertilization experiment. Geoderma 204–205, 84–93.
De Gryze, S., Jassogne, L., Six, J., Bossuyt, H., Wevers, M., Merckx, R., 2006. Pore structure changes during decomposition of fresh residue: X-ray tomography analyses. Geoderma 134, 82–96.
Deurer, M., Grinev, D., Young, I., Clothier, B., Müller, K., 2009. The impact of soil carbon management on soil macropore structure: a comparison of two apple orchard systems in New Zealand. Eur. J. Soil Sci. 60, 945–955.
Doube, M., Kłosowski, M.M., Arganda-Carreras, I., Cordelières, F.P., Dougherty, R.P., Jackson, J.S., Schmid, B., Hutchinson, J.R., Shefelbine, S.J., 2010. BoneJ: free and extensible bone image analysis in Image. J. Bone 47, 1076–1079.
Emerson, W.W., McGarry, D., 2003. Organic carbon and soil porosity. Soil Res. 41, 107–118.
Ersoy, O., Aydar, E., Gourgaud, A., Bayhan, H., 2008. Quantitative analysis on volcanic ash surfaces: application of extended depth-of-field (focus) algorithm for light and scanning electron microscopy and 3D reconstruction. Micron 39, 128–136.
FAO, 1990. Fertilizer Yearbook, 39. FAO, Rome.
Garbout, A., Munkholm, L.J., Hansen, S.B., 2012. The use of PET/CT technique for 3D visualization and quantification of real-time soil/plant interactions. Plant Soil 352, 113–127.
Garbout, A., Munkholm, L.J., Hansen, S.B., 2013a. Temporal dynamics for soil aggregates determined using X-ray CT scanning. Geoderma 204, 15–22.
Garbout, A., Munkholm, L.J., Hansen, S.B., 2013b. Tillage effects on topsoil structural quality assessed using X-ray CT, soil cores and visual soil evaluation. Soil Till. Res. 128, 104–109.
Horn, R., Smucker, A., 2005. Structure formation and its consequences for gas and water transport in unsaturated arable and forest soils. Soil Till. Res. 82, 5–14.
Jiang, J.P., Xiong, Y.C., Jiang, H.M., Ye, D.Y., Song, Y.J., Li, F.M., 2009. Soil microbial activity during secondary vegetation succession in semiarid abandoned lands of Loess Plateau. Pedosphere 19, 735–747.
Kavdır, Y., Smucker, A.J.M., 2005. Soil aggregate sequestration of cover crop root and shoot-derived nitrogen. Plant Soil 272, 263–276.
Kravchenko, A., Wang, A., Smucker, A., Rivers, M., 2011. Long-term differences in tillage and land use affect intra-aggregate pore heterogeneity. Soil Sci. Soc. Am. J. 75, 1658–1666.
Le Bissonnais, Y., 1996. Aggregate stability and assessment of soil crustability and erodibility: I. Theory and methodology. Eur. J. Soil Sci. 47, 425–437.
Li, Y.Y., Shao, M.A., 2006. Change of soil physical properties under long-term natural vegetation restoration in the Loess Plateau of China. J. Arid Environ. 64, 77–96.
Li, X.R., Kong, D.S., Tan, H.J., Wang, X.P., 2007. Changes in soil and vegetation following stabilisation of dunes in the southeastern fringe of the Tengger Desert, China. Plant Soil 300, 221–231.
Ma, R.M., Cai, C.F., Li, Z.X., Wang, J.G., Xiao, T.Q., Peng, G.Y., Yang, W., 2015. Evaluation of soil aggregate microstructure and stability under wetting and drying cycles in two Ultisols using synchrotron-based X-ray micro-computed tomography. Soil Till. Res. 149, 1–11.
Miller, R., Jastrow, J., 1990. Hierarchy of root and mycorrhizal fungal interactions with soil aggregation. Soil Biol. Biochem. 22, 579–584.
Odgaard, A., 1997. Three-dimensional methods for quantification of cancellous bone architecture. Bone 20, 315–328.
Pagliai, M., Vignozzi, N., Pellegrini, S., 2004. Soil structure and the effect of management practices. Soil Till. Res. 79, 131–143.
Park, E.J., Smucker, A.J.M., 2005. Saturated hydraulic conductivity and porosity within macroaggregates modified by tillage. Soil Sci. Soc. Am. J. 69, 38–45.
Peng, X., Zhang, B., Zhao, Q., Horn, R., Hallett, P.D., 2003. Influence of types of restorative vegetation on the wetting properties of aggregates in a severely degraded clayey Ultisol in subtropical China. Geoderma 115, 313–324.
Peng, X., Horn, R., Hallett, P., 2015. Soil structure and its functions in ecosystems: phase matter & scale matter. Soil Till. Res. 146, 1–3.
Perfect, E., Kay, B.D., 1995. Applications of fractals in soil and tillage research: a review. Soil Till. Res. 36, 1–20.
Perret, J.S., Prasher, S.O., Kacimov, A.R., 2003. Mass fractal dimension of soil macropores using computed tomography: from the box-counting to the cube-counting algorithm. Eur. J. Soil Sci. 54, 569–579.
Peth, S., Horn, R., Beckmann, F., Donath, T., Fischer, J., Smucker, A., 2008. Three-dimensional quantification of intra-aggregate pore-space features using synchrotron-radiation-based microtomography. Soil Sci. Soc. Am. J. 72, 897–907.
Pulleman, M.M., Marinissen, J.C.Y., 2004. Physical protection of mineralizable C in aggregates from long-term pasture and arable soil. Geoderma 120, 273–282.
Rasband, W.S, 1997–2014. ImageJ. U.S. National Institutes of Health Bethesda, MD, USA.
Rillig, M.C., Mummey, D.L., 2006. Mycorrhizas and soil structure. New Phytol. 171, 41–53.
Rutigliano, F., D'ascoli, R., De Santo, A.V., 2004. Soil microbial metabolism and nutrient status in a Mediterranean area as affected by plant cover. Soil Biol. Biochem. 36, 1719–1729.

Schmid, B., Schindelin, J., Cardona, A., Longair, M., Heisenberg, M., 2010. A high-level 3D visualization API for Java and ImageJ. BMC Bioinform. 11, 274.
Six, J., Elliott, E.T., Paustian, K., 2000. Soil structure and soil organic matter: II. A normalized stability index and the effect of mineralogy. Soil Sci. Soc. Am. J. 64, 1042–1049.
Six, J., Bossuyt, H., Degryze, S., Denef, K., 2004. A history of research on the link between (micro) aggregates, soil biota, and soil organic matter dynamics. Soil Till. Res. 79, 7–31.
Smucker, A.J.M., Park, E.J., Dörner, J., Horn, R., 2007. Soil micropore development and contributions to soluble carbon transport within macroaggregates. Vadose Zone J. 6, 282–290.
Soil Survey Laboratory Methods Manual. . http://soils.usda.gov/technical/lmm.
Sparling, G., Schipper, L., Bettjeman, W., Hill, R., 2004. Soil quality monitoring in New Zealand: practical lessons from a 6-year trial. Agric. Ecosyst. Environ. 104, 523–534.
Taina, I.A., Heck, R.J., Elliot, T.R., 2008. Application of X-ray computed tomography to soil science: a literature review. Can. J. Soil Sci. 88, 1–19.
Turner, N.C., Li, F.M., Xiong, Y.C., Siddique, K.H.M., 2011. Agricultural ecosystem management in dry areas: challenges and solutions. Plant Soil 347, 1–6.
Wadell, H., 1932. Volume, shape, and roundness of rock particles. J. Geol. 443–451.
Wang, G.H., 2002. Plant traits and soil chemical variables during a secondary vegetation succession in abandoned fields on the Loess Plateau. Acta Bot. Sin. 44, 990–998.
Wang, G.L., Liu, G.B., Xu, M.X., 2009. Above-and belowground dynamics of plant community succession following abandonment of farmland on the Loess Plateau, China. Plant Soil 316, 227–239.
Wang, B., Liu, G.B., Xue, S., Zhu, B., 2011a. Changes in soil physico-chemical and microbiological properties during natural succession on abandoned farmland in the Loess Plateau. Environ. Earth Sci. 62, 915–925.
Wang, W., Kravchenko, A., Smucker, A., Rivers, M., 2011b. Comparison of image segmentation methods in simulated 2D and 3D microtomographic images of soil aggregates. Geoderma 162, 231–241.
Wei, J., Zhou, J., Tian, J.L., He, X.B., Tang, K.L., 2006. Decoupling soil erosion and human activities on the Chinese Loess Plateau in the 20th century. Catena 68, 10–15.
Xue, S., Li, P., Liu, G.B., Li, Z.B., Zhang, C., 2013. Changes in soil hot-water extractable C, N and P fractions during vegetative restoration in zhifanggou watershed on the Loess Plateau. J. Integr. Agric. 12, 2250–2259.
Young, I.M., Crawford, J.W., Rappoldt, C., 2001. New methods and models for characterising structural heterogeneity of soil. Soil Till. Res. 61, 33–45.
Zhang, C., Xue, S., Liu, G.B., Song, Z.L., 2011. A comparison of soil qualities of different revegetation types in the Loess Plateau, China. Plant Soil 347, 163–178.
Zhang, C., Liu, G.B., Xue, S., Zhang, C.S., 2012. Rhizosphere soil microbial properties on abandoned croplands in the Loess Plateau, China during vegetation succession. Eur. J. Soil Biol. 50, 127–136.
Zhang, C., Liu, G.B., Xue, S., Sun, C.L., 2013. Soil organic carbon and total nitrogen storage as affected by land use in a small watershed of the Loess Plateau. China. Eur. J. Soil Biol. 54, 16–24.
Zhao, S.W., Zhao, Y.G., Wu, J.S., 2010. Quantitative analysis of soil pores under natural vegetation successions on the Loess Plateau. Sci. China Earth Sci. 53, 617–625.
Zhou, H., Peng, X., Peth, S., Xiao, T.Q., 2012. Effects of vegetation restoration on soil aggregate microstructure quantified with synchrotron-based micro-computed tomography. Soil Till. Res. 124, 17–23.
Zhou, H., Peng, X.H., Perfect, E., Xiao, T.Q., Peng, G., 2013. Effects of organic and inorganic fertilization on soil aggregation in an Ultisol as characterized by synchrotron based X-ray micro-computed tomography. Geoderma 195-196, 23–30.